Accepted Manuscript

Optical properties of amorphous and crystalline tris(8-hydroxyquinoline) indium films

E.M. El-Menyawy

PII: S0925-8388(16)31454-2

DOI: 10.1016/j.jallcom.2016.05.121

Reference: JALCOM 37641

To appear in: *Journal of Alloys and Compounds*

Received Date: 12 December 2015

Revised Date: 26 April 2016

Accepted Date: 13 May 2016

Please cite this article as: E.M. El-Menyawy, Optical properties of amorphous and crystalline tris(8-hydroxyquinoline) indium films, *Journal of Alloys and Compounds* (2016), doi: 10.1016/j.jallcom.2016.05.121.

Optical properties of amorphous and crystalline tris(8-hydroxyquinoline) indium films

E.M. El-Menyawy
Solid State Electronics Laboratory, Solid State Physics Department, Physical Research Division, National Research Centre, 33 El-Bohouth St., Dokki, Giza 12622, Egypt.

Abstract

Tris(8-hydroxyquinoline) indium (Inq_3) films were physically deposited via thermal evaporation technique and were subsequently thermally annealed at different temperatures in air atmosphere. The effect of annealing on the structural and optical properties of the films was investigated. X-ray diffraction showed that the as-deposited and annealed films at 100 and 200 ˚C have amorphous structure, whereas the annealed films at 270 and 300 ˚C have crystalline structure in which a preferred orientation of growth is obtained. The evolution of the optical properties of the films due to annealing has been correlated with their structural properties. The optical properties were studied in terms of spectrophotometeric measurements of the transmittance and reflectance over the spectral range 200-2500 nm, from which the refractive and absorption indices were calculated using Murmann's exact equations. The single oscillator and Drude models were applied for determining the dispersion parameters of the films. Analysis of the absorption coefficient revealed that the films have direct allowed optical band gap of 2.77 *eV*, which is increased to 2.85 *eV* as a result of annealing. The thermal properties were studied by means of differential scanning calorimetry and thermogravimetric measurements.

Keywords: Inq_3 films; Structural properties; Optical constants; Annealing.

Corresponding author: Tel: +2 01006021326; Fax: +2 0233709310.

E-mail address: emad_elmenyawy@yahoo.com (E.M. El-Menyawy).

1. Introduction

Organic semiconductors with promising optical and electrical properties are recognized as an important class of interesting materials for applications in advanced electronic and optoelectronic devices in which their physical properties can be tuned by chemical modification on the molecular frame. The domain of organic materials continues to be of great scientific and commercial interest due to other advantages such as low cost and ease of processing. They are currently used as active layers in large number of advanced electronic and optoelectronic devices such as light emitting diodes [1], thin film transistors [2] and solar cells [3], as alternatives to expensive inorganic materials.

Tris(8-hydroxyquinoline) aluminum (Alq_3) is the first efficient material in organic light emitting diode (OLED) devices, which was reported in 1987 by Tang and Vanslyke [4]. Since then, intense efforts have been dedicated to develop and improve the efficiency of such diodes. Most of the recent studies have been directed towards improving morphological stability [5], optimizing the device characteristics [6], understanding the charge carrier transport mechanisms [7] and tuning the emission spectrum of OLED [8]. Besides, Alq_3 is used as a buffer electron transport layer [9] and dopant material in organic solar cells [10]. Ever since the success of Alq_3 in these devices, a lot of attention has been paid to synthesize and investigate other counterparts. In this regard, Inq_3 has been introduced as promising candidate in OLEDs. Triggered by its interesting properties, efforts have been paid for further material analysis and characterization. The study of the optical behavior of such materials in thin film form is a prerequisite for the successful device fabrication. Shukla and Kumar [11] have been investigated the optical properties of Inq_3 and Alq_3 films by using spectroscopic ellipsometry. The study showed that the refractive index of Inq_3 films is higher than Alq_3 films. Thangaraju et al. [12] showed that the Inq_3 films have less photoluminescence intensity compared with that of Alq_3 thin film. Thermal annealing was used as an effective tool for influencing the structural and optical properties of Alq_3 [13-15] and Gaq_3 [16] films.

To the best of my knowledge, the effect of thermal annealing on the structural and optical properties of Inq_3 thin films has not been extensively reported. The target of this work is to study the influence of thermal annealing temperature on the structural properties and optical functions of thermally evaporated Inq_3 films over the spectral range 200-2500 nm. Thermal annealing is a common used process in optical applications, which is helpful tool to improve the film properties. For example, annealing has been used as a vital process to improve the electrical conversion efficiency of solar cells. Thus, it is important to find the optimum annealing temperature, at which the film could possess better optical properties.

2. Experimental

2.1 Synthesis

Tris(8-hydroxyquinoline) indium was prepared according the procedure given elsewhere [17]. In typical synthesis, 0.5 g of 8-hydroxyquinoline was dissolved in a mixture of 10 ml double distilled water and 2.5 ml of glacial acetic acid. The mixture was vigorously stirred until an orange transparent solution was obtained. Then, 0.3 g of indium nitrate hydrate was dissolved in 20 ml of double distilled water and stirred until a clear solution was obtained. The two solutions were mixed together and stirred for 5 min. After that, ammonium hydroxide was added to the mixture solutions, drop by drop with continuous stirring to get maximum precipitation. A yellow-green precipitate was filtered out and washed 15 times with double distilled water and dried at 80 ˚C under argon gas flow.

2.2 Films deposition and measurements

Inq_3 films were deposited onto pre-cleaned glass and optically flat fused quartz substrates using thermal evaporation technique under a base pressure of about 10^{-4} Pa by using high vacuum coating unit (Edwards, E 306 A). Initially, Inq_3 powder was placed inside a quartz crucible that has been surrounded by a tungsten coil capable of supplying sufficient heat to the materials upon passing an electrical current through this coil. Current of about 40 A was enough to start sublimating Inq_3 powder. The rate of deposition and film thickness were controlled during the evaporation by using a quartz crystal thickness monitor. The rate of deposition was adjusted at 0.15 nm/s. The film thickness was determined as 386 nm after deposition by spectrophotometeric method. The substrates were kept at room temperature (25 ˚C) during the deposition process. Prior to deposition, the substrates were cleaned ultrasonically for 15 min with hot distilled water, followed by 10 min rinsing in an ultrasonic bath in acetone, ethanol and distilled water, respectively. Finally, the substrates were dried thoroughly under argon gas. Glass substrates were used for structural analysis, whereas quartz substrates were used for optical measurements.

Inq_3 films were thermally annealed at temperatures of 100, 200, 270 and 300 ˚C in air atmosphere. Annealing was performed in dark condition and the time of annealing was two hours. The temperature of the samples was recorded by using NiCr-NiAl thermocouple with an accuracy of ±1 ˚C.

The X-ray diffractometer (Philips X' pert) with Ni-filtered CuK_α-radiation was used to identify the structural characteristics of both powder and films. The measurements were performed in the diffraction angle (2θ) range 4–80˚ with a step size of 0.02 (2θ/s). Morphology of the films was studied by field emission scanning electron microscope (Quanta FEG 250).

The optical transmittance and reflectance spectra of the films were recorded over the wavelength range 200–2500 nm using double beam spectrophotometer (JASCO V-570 UV–Vis–NIR). The measurements were performed under ambient conditions. The absolute values of total measured transmittance, T_m, after introducing corrections resulting from the absorbance and reflectance of the substrate were calculated by [18]:

$$T = T_m\left(1 - R_q\right) \tag{1}$$

where R_q is the reflectance of reference quartz substrate. The spectrophotometer was also provided with a reflection attachment to measure the reflectance. The absolute values of the total measured reflectance, R_m, after introducing corrections resulting from reflectance of the substrate and reference mirror were calculated by:

$$R = R_m R_{Al}\left\{1 + (1 - R_q)^2\right\} - T^2 R_q \tag{2}$$

where R_{Al} is the reflectance of the reference aluminum mirror.

The thermogravimetric (TG) and differential scanning calorimetry (DSC) measurements were performed at heating rate of 10 ˚C/min and in nitrogen environment by thermogravimetric analyzer SDTQ 600 TA.

3. Results and discussion

3.1 Structural properties

Fig. 1 depicts the X-ray diffraction patterns of Inq_3 in both powder and thin film conditions. It can be observed that the spectrum of the powder has different peaks with different intensities implying polycrystalline structure. Upon thermal deposition, no identified diffraction peaks are found which give the ambiguous evidence of amorphous structure. The same behavior can also be seen for annealed films at 100 and 200 ˚C. Upon rising annealing temperature up to 270 ˚C, a preferred orientation of growth along the diffraction peak centered at diffraction angle of 7.03˚ is obtained indicating crystalline structure. The intensity of this peak is slightly increased by annealing at 300 ˚C indicating slight improvement of films crystallinity. The appearance of this diffraction peak at high annealing temperatures is attributed to the sufficient increase in supply of thermal energy for crystallization, re-crystallization and growth of grains in the films. As-deposited Alq_3 [13] and Gaq_3 [16] films are also found to grow with amorphous structure. Thermal annealing at 200 ˚C is found to crystallize Alq_3 films and thermal annealing at 255 ˚C is found to crystallize Gaq_3 films.

The surface morphology of films plays an important role for electronic and optoelectronic device applications. Surface morphology of Inq_3 films is investigated by field emission scanning electron microscope (FESEM). Fig. 2(a,b) represents the FESEM images of as-deposited and annealed films at 270 ˚C with the same value of magnification. The SEM image shows that the particles of as-deposited amorphous films have granular shape with uniform of distribution over the substrate surface. With annealing, some of irregular shaped particles in the as-deposited film are transformed to a more rounded structure resulting in more defined particles which can be attributed to crystallization process.

3.2 Optical properties

Inq_3 films were thermally annealed at different temperatures (100, 200, 270 and 300 ˚C). The effect of thermal annealing at 100 and 200 ˚C on the transmittance and reflectance spectra of the films was very weak. The attempt for measuring the transmittance and reflectance of the annealed films at 300 ˚C has failed, because that the annealing was resulted in a decrease in film thickness and formation of rough surface. So, the influence of thermal annealing on the optical properties of the films is achieved at only 270 ˚C.

Fig. 3 demonstrates the optical transmittance and reflectance spectra of as-deposited and annealed Inq_3 films. Inspection of this figure shows that the spectra of as-deposited films can be simply divided into two regions. In spectral range 200-550 nm, the total sum of T and R is less than unity implying the existence of absorption. At wavelengths greater than 550 nm, the total sum of T and R approaches unity value i.e transparent region. The absorption region is separated from transparent one by sharp transmittance edge. In the transparent region, the T and R spectra of the films exhibit many peaks and valleys. These oscillations are due to the interference effect originating from the multiple reflections which occur at the interface of the air-film and film-substrate systems, constructive and destructive wave interference occur periodically. On annealing, the transmittance edge is slightly shifted towards shorter wavelengths. The value of T in transparent region is also decreased and the corresponding value of R is increased. It can be observed that the T and R spectra of as-deposited and annealed films have nearly the same behavior in transparent region. This indicates that the as-deposited and annealed film have almost the same thickness, within the experimental error.

The optical transmittance and reflectance spectra of Inq_3 films were used to estimate the refractive, *n*, and absorption, *k*, indices using Murmann′s equations [19,20]. To get the optical constants, *n* and *k*, a computer program comprising a modified search technique of Abèlès et al. technique [21] was used. The idea of technique is based on minimizing $|\Delta T|^2$ and $|\Delta R|^2$ simultaneously, where

$$|\Delta T|^2 = |T_{(n,k)} - T|^2 \quad (3)$$

$$|\Delta R|^2 = |R_{(n,k)} - R|^2 \quad (4)$$

where *T* and *R* are the experimental absolute values calculated from Eqs (1) and (2), respectively. $R_{(n,k)}$ and $T_{(n,k)}$ are the proposed values of *T*, *R* using Murmann′s equations. By applying such technique, values of *n* and *k* are obtained. The details of these calculations are given in previous work [22].

The spectral distributions of the calculated refractive index, *n*, of as-deposited and annealed Inq_3 films are depicted in Fig. 4. It can be seen that the spectrum of as-deposited films exhibits three peaks located at 280, 330 and 440 nm. These peaks represent the anomalous dispersion of the refractive index which can be explained with the multi-oscillator model [23]. At wavelength range 550-2500 nm, the refractive index decreases with increasing the wavelength and shows non-dispersive behavior at higher wavelengths. This behavior is the normal dispersion which can be interpreted by using single oscillator model. The value of the refractive index for as-deposited films is in the range of 1.9-2 which is slightly higher than that observed for Alq_3 [24]. With annealing, the refractive index increases over the whole spectral range and the peak located at 440 nm shifts slightly towards higher wavelengths.

Fig. 5 illustrates the influence of annealing on the absorption index spectra of Inq_3. The spectrum of the as-deposited film is dominated by two major bands in ultraviolet and visible spectral regions. Similar behavior is also observed for Alq_3 [25] and Gaq_3 [26]. Muhammad et al. [26] have been pointed that the band in the visible light region is attributed to the optoelectronic transition across π-π* orbitals, whereas that the band in the ultraviolet region is due to the optoelectronic transition from 4*p* to π* orbital. Inspection of the absorption spectra shows that the intensity of the absorption band in the visible light region is decreased by annealing, whereas the intensity of the absorption band in the ultraviolet region is increased. In addition, the visible light absorption band shifts towards higher energy, while the ultraviolet absorption band shifts towards lower energy. From the foregoing observations, it can be deduced that the changes in the optical constants of Inq_3 films as a result of annealing are attributed to corresponding enhancement in both packing density and intermolecular interactions upon crystallization or rearrangement [27].

In weak absorption region, the dispersion data of the refractive index can be evaluated according to the single oscillator model proposed by Wemple and Di Domenico [28,29]. According to this model, the real part of dielectric function, ε_1, is expressed by:

$$\varepsilon_1 = n^2 - k^2 = 1 + \frac{E_d E_o}{E_o - (h\nu)^2} \tag{5}$$

where E_d and E_o are the dispersion and oscillator energies, respectively and $h\nu$ is the photon energy. The parameter E_d is a measure of the intensity of inter-band optical transitions and it does not depend significantly on the band gap, while E_o can be considered as an average value of the energy gap of the material. Fig. 6 shows the relation between $(n^2\text{-}1)^{-1}$ and $(h\nu)^2$ for as-deposited and annealed Inq_3 films. The relation gives a straight line over a long range of photon energy verifying Eq. 5. The deviation from linearity at low photon energy is observed which can be ascribed to the negative contribution of lattice vibration to the refractive index [29]. The values of E_d and E_o of as-deposited and annealed Inq_3 films are determined from the slope $(1/E_\mathrm{d}E_\mathrm{o})$ and the intercept $(E_\mathrm{o}/E_\mathrm{d})$ of the straight lines. The values of E_d and E_o for as-deposited films are estimated as 15.06 and 5.56 *eV*, respectively. With annealing, these values are increased to 27.94 and 7.73 *eV*, respectively. The dielectric constants at high frequency $(\varepsilon_\infty = n_\infty^2)$ were determined from the intercept of the straight line with the $(n^2\text{-}1)^{-1}$ axis at zero photon energy. The value of ε_∞ for as-deposited and annealed films was determined as 3.71 and 4.61, respectively.

The real part of the dielectric function can be analyzed to obtain additional information concerning the contribution of the free carriers and the lattice vibration modes to the dispersion. The dependence of the real part of the dielectric function relation on the wavelength of the incident light is expressed by [30]:

$$\varepsilon_1 = n^2 - k^2 = \varepsilon_L - \frac{e^2}{4\pi^2 \varepsilon_o c^2} \frac{N}{m^*} \lambda^2 \tag{6}$$

where ε_L is the lattice dielectric constant, e is the charge of the electron, ε_o is the dielectric constant of free space, c is the velocity of light in free space and N/m^* is the ratio of the carrier concentration to its effective mass. Fig. 7 shows the variation of n^2 with λ^2 for the as-deposited and annealed Inq_3 films. The relation shows linear behavior at higher wavelengths. Extrapolating the linear portions to zero wavelength value gives the value of ε_L, whereas the ratio N/m^* is determined from the slope of the straight line portions. The value of ε_L is estimated as 3.72 for as-deposited films and it is increased to 4.63 as a result of annealing. The accordance between the values of ε_L and ε_∞ indicates that the contribution of the free carries is marginal for the films under investigation [31]. Besides, the ratio N/m^* is slightly increased from 1.35×10^{55} to 1.47×10^{55} $Kg^{-1}\ m^{-3}$ by annealing. The value of N/m^* is in the same order of that obtained for Alq_3 [13]. The increase in the ratio N/m^* is due to the crystallinity improvement of the films.

The absorption coefficient of the films was calculated by the well-known relation; $\alpha=4\pi k/\lambda$. According to electronic inter-band absorption theory, optical band gap of non metallic films can be evaluated using Tauc's relation [32]:

$$\alpha h\nu = B\left(h\nu - E_g\right)^m \tag{7}$$

where B is the probability parameter for the transition, E_g is the optical band gap of the material and m is the transition coefficient. The exponent m takes the values 1/2 and 3/2 for direct allowed and forbidden transitions, respectively, and takes the values 2 and 3 for indirect allowed and forbidden transitions, respectively. The experimental data were fitted to different values of m, and it was found that the m=1/2 provided the best fit to the data. This indicates the existence of direct electronic transitions between the molecular orbital energy bands. The relation between $(\alpha h\nu)^2$ and photon energy is represented in Fig. 8. The extrapolation of the straight line graphs $(\alpha h\nu)^2$ =0 gives the values of the optical band gap. The value of E_g is estimated as 2.77 and 2.85 eV for as-deposited and annealed films, respectively. The E_g value is lower than that of Gaq_3 (2.81 eV) and Alq_3 (2.86 eV) films [33] which can be attributed to the effect electrons number in the outer shell for the central metal cation. The increase in the E_g value can be correlated with the improvement of the films crystallinity. The value of the optical band gap of as-deposited and annealed films verifies the relation; $E_o \approx 2 \times E_g$ which is also observed to be verified for Alq_3 [34].

The behavior of the absorption coefficient in the low energy range was found to follow the exponential law given by Urbach's expression [35]:

$$\alpha = \alpha_o \exp\left(\frac{h\nu}{E_U}\right) \qquad \text{for } h\nu < E_g \tag{8}$$

where α_o is a constant, and E_U is an empirical parameter, which has the dimensions of energy and describes the width of the localized states in the band gap. Fig. 9 gives ample evidence that the experimental data below the E_g verifies Eq. 8. From the slopes of this linear relationship, the empirical parameter E_U for as-deposited and annealed films was estimated as 0.16 and 0.14 eV, respectively. These results indicate that as-deposited films have higher values of localized states than the annealed films which are in accordance with the X-ray studies.

Fig. 10 depicts the TG-DSC curves of as-prepared Inq_3 powder. The TG curve shows a weight loss starts at 39 up to about 49 ˚C which is accompanied with endothermic peak in DSC curve. This peak is attributed to the evaporation of the residual ammonium hydroxide. The curves show also that the absorbed water molecules start to evaporate at 85 ˚C and continue to 109 ˚C. The glass transition temperature, T_g, is observed at 198 ˚C and recrystallization temperature, T_c, is located at 261 ˚C. The endothermic peak observed at 375 ˚C is corresponding to the melting point, T_m, whereas that observed at 425 ˚C is corresponding to the degradation temperature, T_d. The values of T_g, T_c and T_m are reported as 177, 251 and 419 ˚C, respectively, for Alq_3 [36] and are determined as 182, 259 and 286 ˚C, respectively, for Gaq_3 [16]. In comparison to Alq_3 and Gaq_3, Inq_3 shows higher thermal stability which can be ascribed to the stabilizing effect of cationic In^{+3} central metal atom [26].

4. Conclusion

Inq_3 powder has polycrystalline structure. As-deposited and thermally annealed films at 100 and 200 ˚C have amorphous structure. Annealing at 270 and 300 ˚C results in crystalline films in which a preferred orientation of growth is observed. Inq_3 films are optically absorbing over the spectral range 200-550 nm, whereas they are optically transparent over the spectral range 550-2500 nm. The refractive index is found to increase with annealing at 270 ˚C. The behavior of the refractive index is investigated in which some important dispersion parameters; E_d, E_o, ε_∞, ε_L and N/m^* are estimated for as-deposited and annealed films. The absorption analysis of the as-deposited films revealed the existence of direct allowed transition with optical energy gap of 2.77 *eV*. This value is increased to 2.85 *eV* due to annealing. Using Urbach's relation, the width of the localized states in the band gap of the films is found to decrease with annealing. Thermal properties analysis showed that Inq_3 has glass transition and recrystallization temperatures of 198 and 261 ˚C, respectively. It could be concluded that the modification in optical properties of the films by annealing is due to crystallization.

References

[1] X-W. Zhang, J-W. Xu, H-R. Xu, H-P. Lin, J. Li, X-Y. Jiang, Z-L. Zhang, Opt. Laser Technol 45 (2013) 181.

[2] J. Lee, J.S. Park, B-L. Lee, J-l. Park, J.W. Chung, S. Lee, Org. Electron. 15 (2014) 2021.

[3] S. Albrecht, B. Grootoonk, S. Neubert, S. Roland, J. Wördenweber, M. Meier, R. Schlatmann, A. Gordijn, D. Neher, Sol. Energy Mater. Sol. Cells 127 (2014) 157.

[4] C.W. Tang, S.A. Vanslyke, Appl. Phys. Lett. 51 (1987) 913.

[5] L.M. Do, E.M. Han, N. Yamamoto, M. Fujihira, Thin Solid Films 273 (1996) 202.

[6] J. McElvain, H. Antoniadis, M.R. Hueschen, J.N. Miller, D.M. Roitman, J.R. Sheat, R.L. Moon, J. Appl. Phys. 80 (1996) 6002.

[7] P.W.M. Blom, M.J.M. de Jong, M.G. van Munster, Phys. Rev. B 55 (1997) 656.

[8] T.A. Hopkins, K. Meerholz, S. Shaheen, M.L. Anderson, A. Schmidt, B. Kippelen, A.B. Padias, H.K. Hall Jr., N. Peyghambarian, N.R. Armstrong, Chem. Mater. 8 (1996) 344.

[9] P. Vivo, J. Jukola, M. Ojala, V. Chukharev, H. Lemmetyinen, Sol. Energy Mater. Sol. Cells 92 (2008) 1416.

[10] P.C. Kao, S.Y. Chu, H.H. Huang, Z.L. Tseng, Y. Ch. Chen, Thin Solid Films 517 (2009) 5301.

[11] V.K. Shukla, S. Kumar, Opt. Mater. 29 (2007) 1809.

[12] K. Thangaraju, R. Kumaran, P. Ramamoorthy, V. Narayananc, J. Kumar, Optik 123 (2012) 1393.

[13] M.M. El-Nahass, A.M. Farid, A.A. Atta, J. Alloys Compd. 507 (2010) 112.

[14] G. Baldacchini, T. Baldacchini, P. Chiacchiaretta, R. B.Pode, Q.-M. Wang, J. Lumin. 129 (2009) 1831.

[15] M. Cuba, G. Muralidharan, Luminescence 30 (2015) 352.

[16] F.F. Muhammad, K. Sulaiman, Mater. Chem. Phys. 129 (2011) 1152.

[17] E.M. El-Menyawy, Mater. Sci. Semicond. Process. 32 (2015) 145.

[18] E.M. El-Menyawy, A.A. Elagamey, S.R. Elgogary, R.A.N. Abu El-Enein, Spectrochim. Acta, Part A 108 (2013) 75.

[19] O.S. Heavens, in: G. Hass, R. Thus (Eds.), Physics of Thin Films, Academic, New York, 1964, p. 193.

[20] H.M. Liddeli, in: Computer-Aided Technique for the Design of Multilayer Filters, Hilger, Bristol, 1981 p. 118.

[21] F. Abèlès, M.L. Thèyè, Surf. Sci. 5 (1966) 325.

[22] H.M. Zeyada, M.M. El-Nahass, I.K. El-Zawawi, E.M. El-Menyawy, J. Phys. Chem. Solids 71 (2010) 867.

[23] A. Stendal, U. Beckers, S. Willbrand, O. Stenzel, C.V. Borczyskowski, J. Phys. B: Atomic. Mol. Opt. Phys. 29 (1996) 2589.

[24] A. Zawadzka, P. Płóciennik, J. Strzelecki, Z. Łukasiak, B. Sahraoui, Opt. Mater. 36 (2014) 91.

[25] A.B. Djurišiċ, C.Y. Kwong, W.L. Guo, T.W. Lau, E.H. Li, E.H. Liu, H.S. Kwok, L.S.M. Lam, W.K. Chan, Appl. Phys. A 78 (2004) 375.

[26] F.F. Muhammad, A.I.A. Hapip, K. Sulaiman, J. Organomet. Chem. 695 (2010) 2526.

[27] I. Hernández, W.P. Gillin, J. Phys. Chem. B 113 (2009) 14079.

[28] S.H. Wemple, M. DiDomenico Jr., Phys. Rev. B 3 (1971) 1338.

[29] S.H. Wemple, Phys. Rev. B 7 (1973) 3767.

[30] M.M. El-Nahass, E.M. El-Menyawy, Mater. Sci. Eng., B 177 (2012) 145.

[31] M.M. El-Nahass, F.S.H. Abu-Samaha, S. Menshawy, E. Elesh, Opt Laser Technol 64 (2014) 28.

[32] J. Tauc, A. Menth, J. Non-Cryst. Solids 8–10 (1972) 569.

[33] F.F. Muhammad, K. Sulaiman, Measurement 44 (2011) 1468.

[34] Z.Z. You, G.J. Hua, Vacuum 83 (2009) 984.

[35] F. Urbach, Phys. Rev. 92 (1953) 1324.

[36] L.S. Sapochak, A. Padmaperuma, N. Washton, F. Endrino, G.T. Schmett, J. Marshall, D. Fogarty, P. E. Burrows, S. R. Forrest, J. Am. Chem. Soc. 123 (2001) 6300.

Figure captions

Scheme 1 Molecular structure of Inq_3 compound.

Fig. 1 X-ray diffraction spectra of Inq_3: (a) powder, (b) as-deposited film, (c) annealed films at 100 ˚C, (d) annealed films at 200 ˚C, (e) annealed film at 270 ˚C and (f) annealed film at 300 ˚C.

Fig. 2 SEM images of Inq_3 films: (a) as-deposited and (b) annealed at 270 ˚C.

Fig. 3 Optical transmittance and reflectance spectra of Inq_3 thin films.

Fig. 4 Refractive index dispersion curve of Inq_3 films.

Fig. 5 Spectral distribution of absorption index for Inq_3 films.

Fig. 6 The relation between $(n^2\text{-}1)^{-1}$ and $(h\nu)^2$ for as-deposited and annealed Inq_3 films.

Fig. 7 The variation of n^2 with λ^2 for as-deposited and annealed Inq_3 films.

Fig. 8 The relation between $(\alpha h\nu)^2$ and photon energy for Inq_3 films.

Fig. 9 The relation between $\ln\alpha$ and $h\nu$ for as-deposited and annealed Inq_3 films.

Fig. 10 TGA-DSC curves of Inq_3 powder.

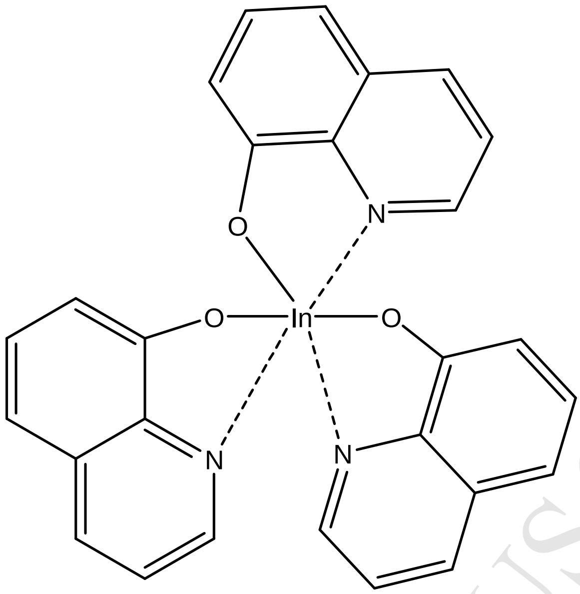

Scheme 1

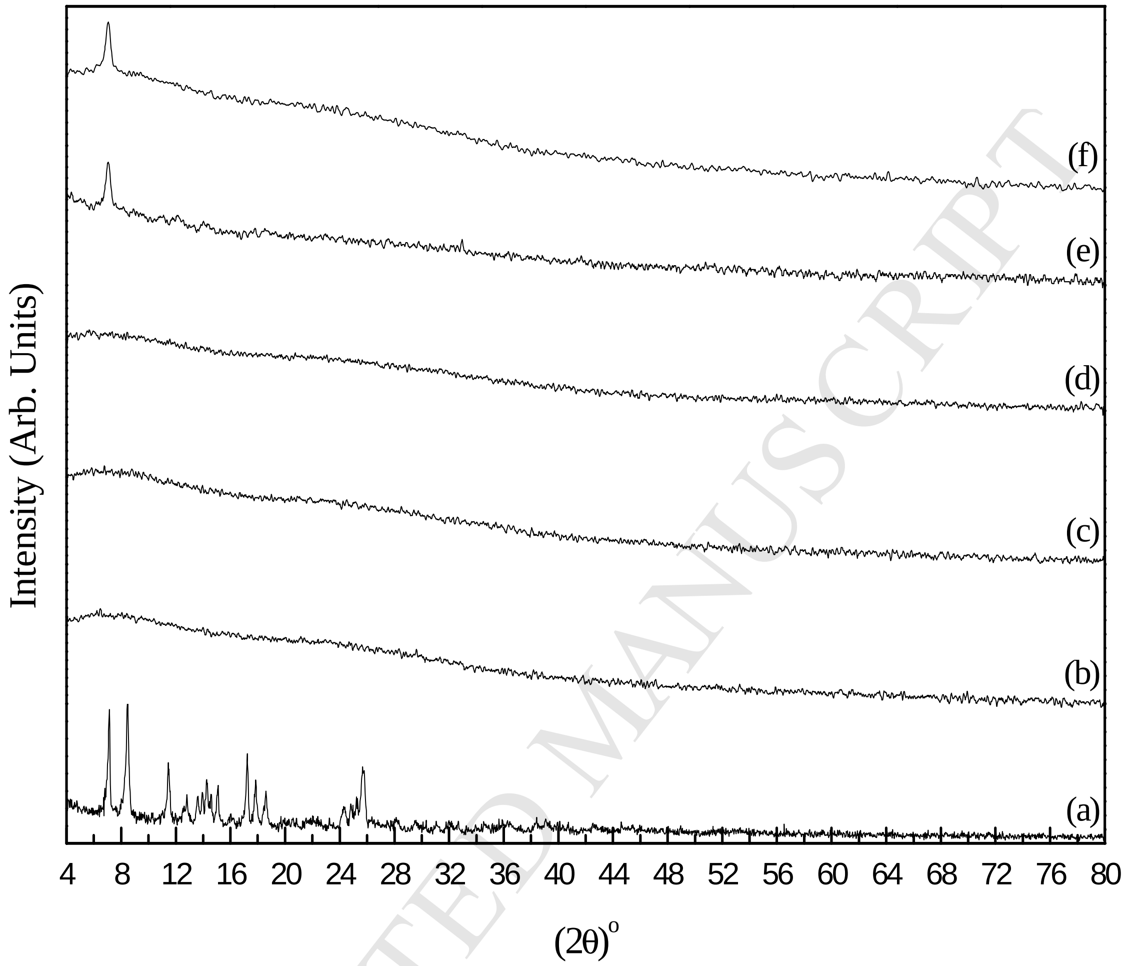
Intensity (Arb. Units)
(f)
(e)
(d)
(c)
(b)
(a)
4 8 12 16 20 24 28 32 36 40 44 48 52 56 60 64 68 72 76 80
(2θ)°

Fig. 1

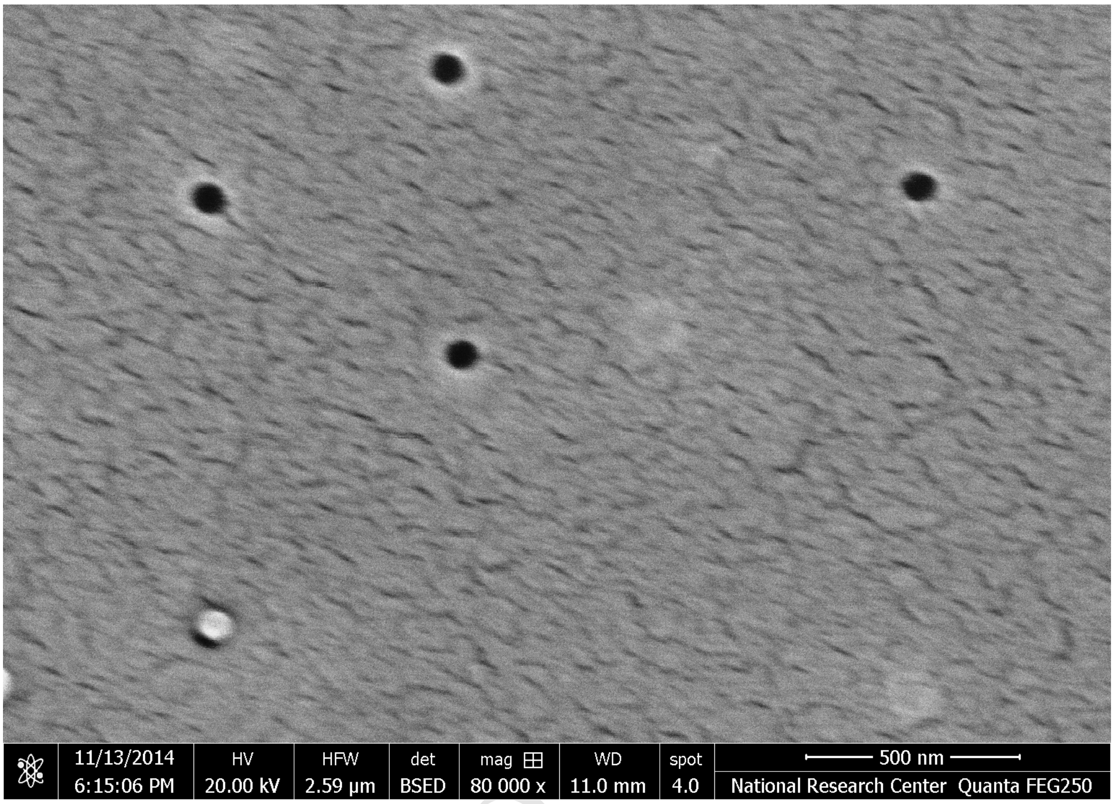
11/13/2014
6:15:06 PM
HV
20.00 kV
HFW
2.59 µm
det
BSED
mag
80 000 x
WD
11.0 mm
spot
4.0
500 nm
National Research Center Quanta FEG250

(a)

(b)

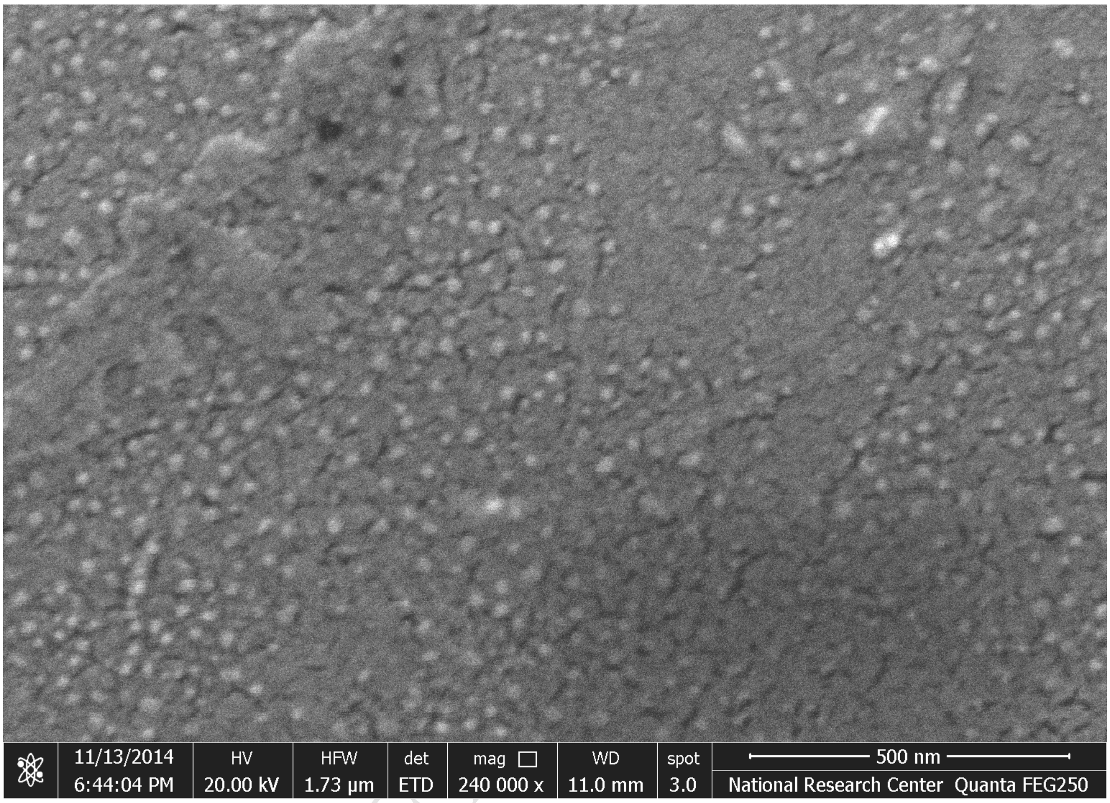
11/13/2014
6:44:04 PM
HV
20.00 kV
HFW
1.73 µm
det
ETD
mag
240 000 x
WD
11.0 mm
spot
3.0
500 nm
National Research Center Quanta FEG250

Fig. 2

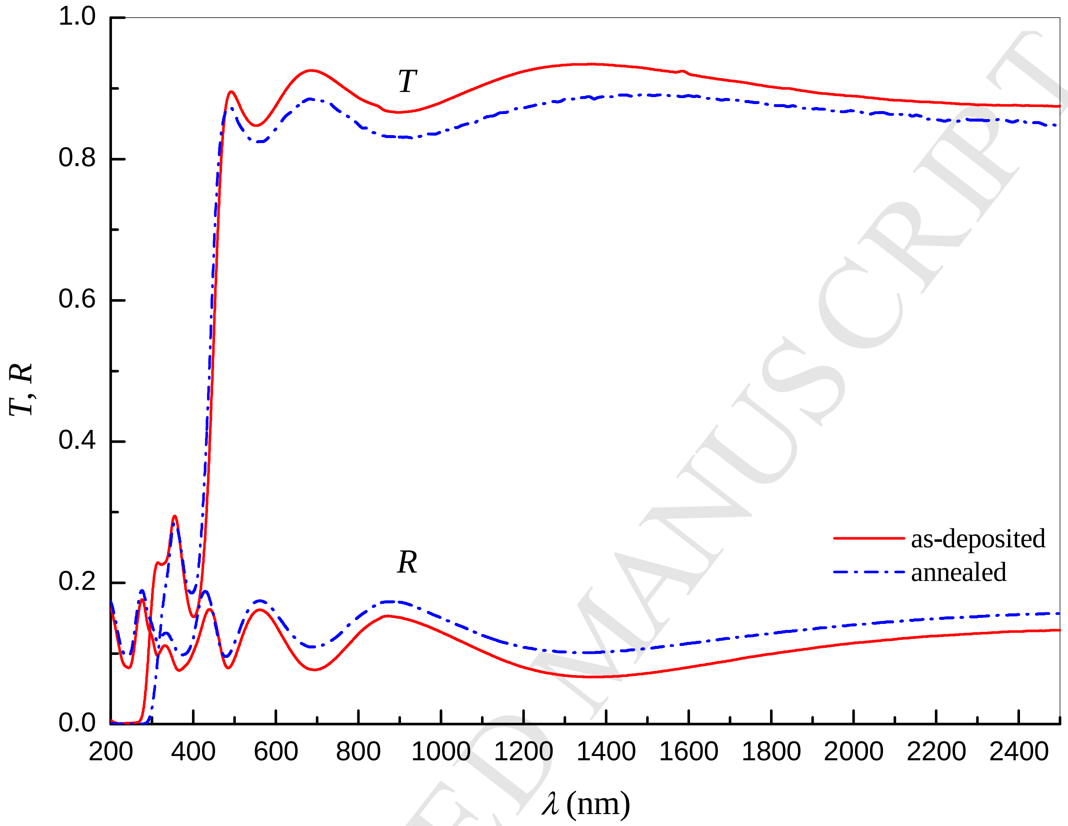
1.0
0.8
0.6
0.4
0.2
0.0
T, R
T
R
as-deposited
annealed
200
400
600
800
1000
1200
1400
1600
1800
2000
2200
2400
λ (nm)

Fig. 3

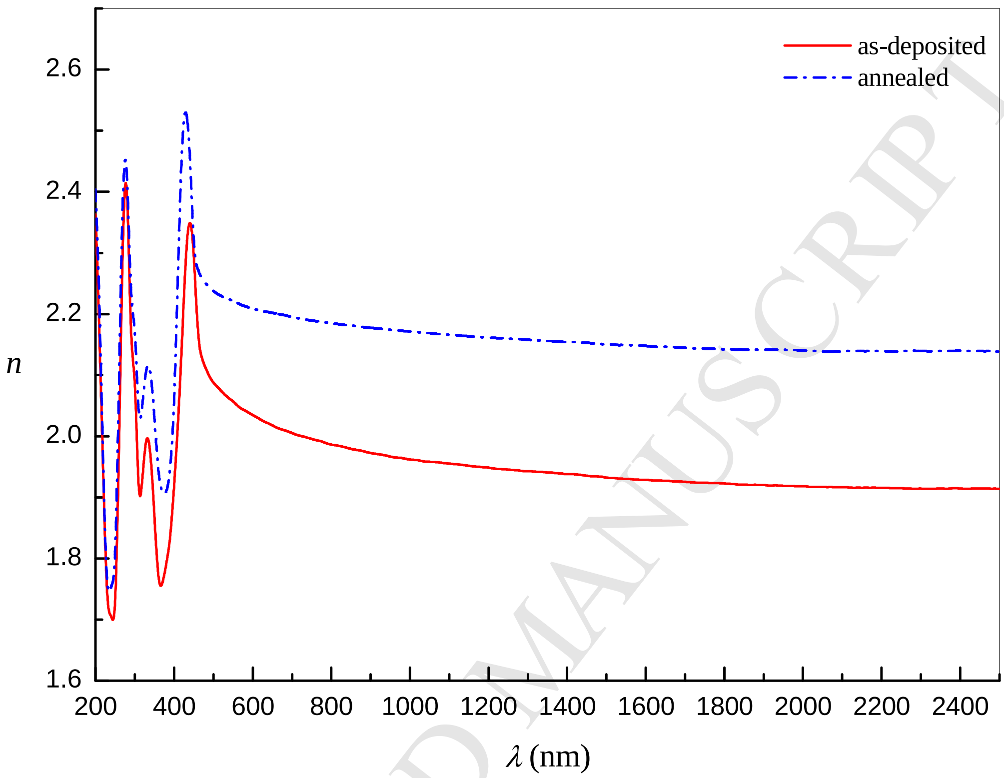

as-deposited
annealed
2.6
2.4
2.2
2.0
1.8
1.6
n
200
400
600
800
1000
1200
1400
1600
1800
2000
2200
2400
λ (nm)

Fig. 4

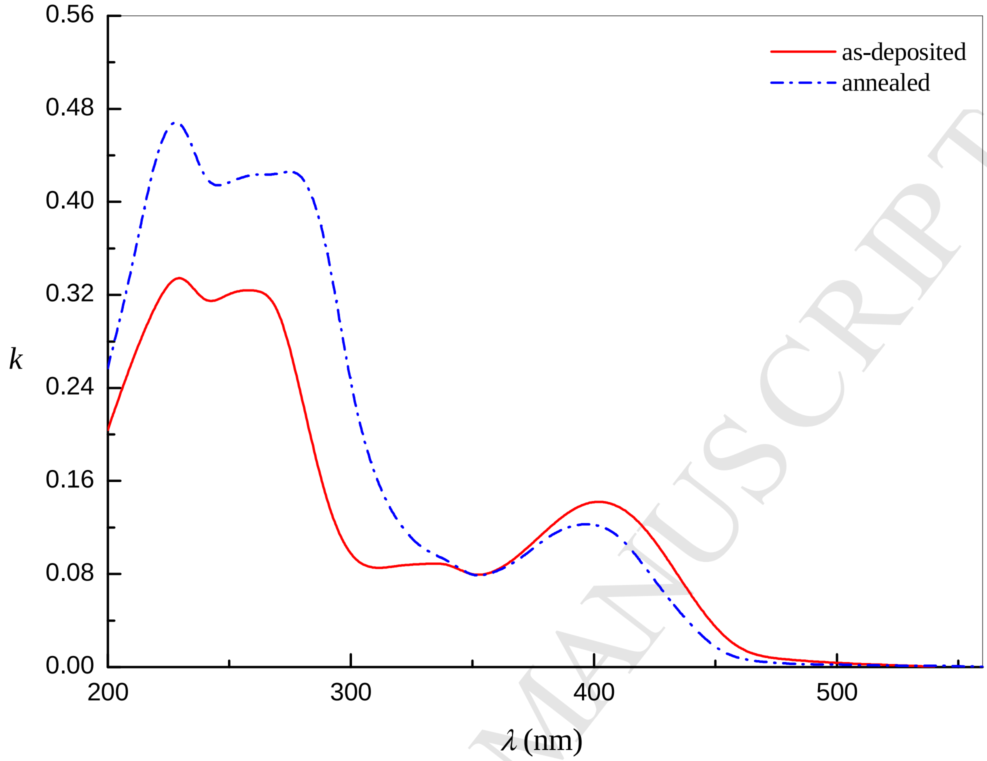
0.56
0.48
0.40
0.32
0.24
0.16
0.08
0.00
k
200
300
400
500
λ (nm)
as-deposited
annealed

Fig. 5

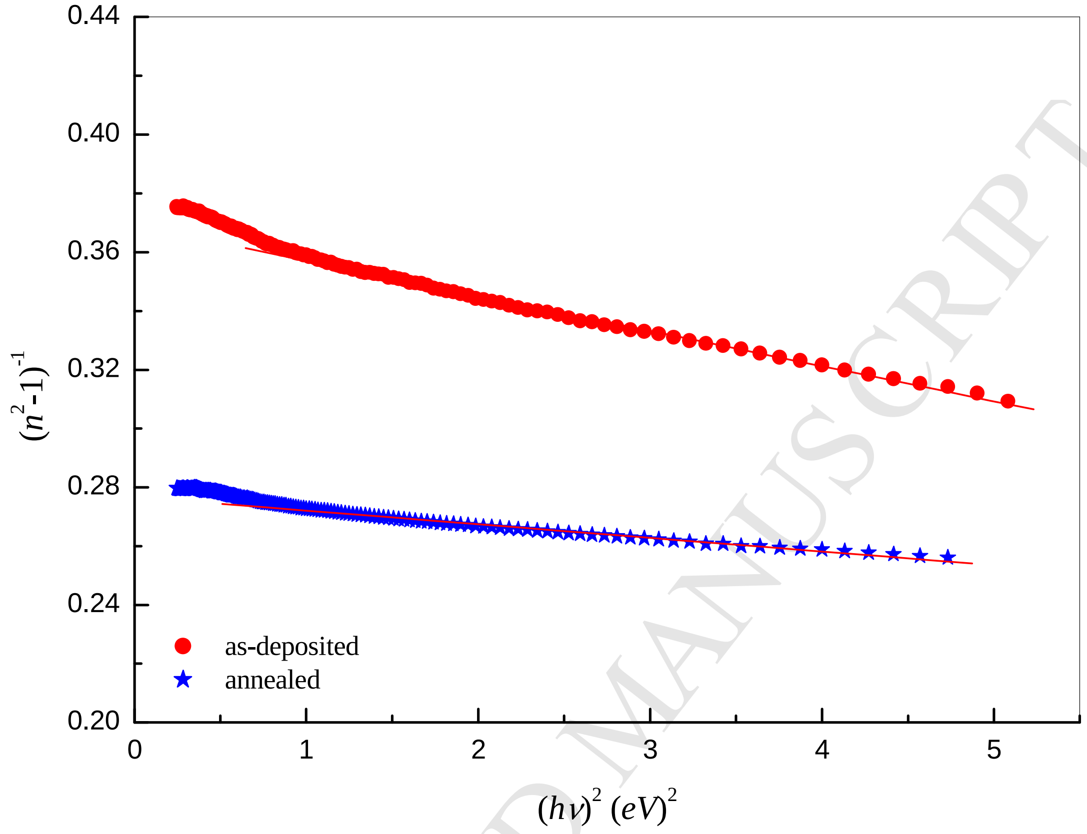
0.44
0.40
0.36
0.32
0.28
0.24
0.20
$(n^2-1)^{-1}$
0
1
2
3
4
5
$(h\nu)^2$ $(eV)^2$
as-deposited
annealed

Fig. 6

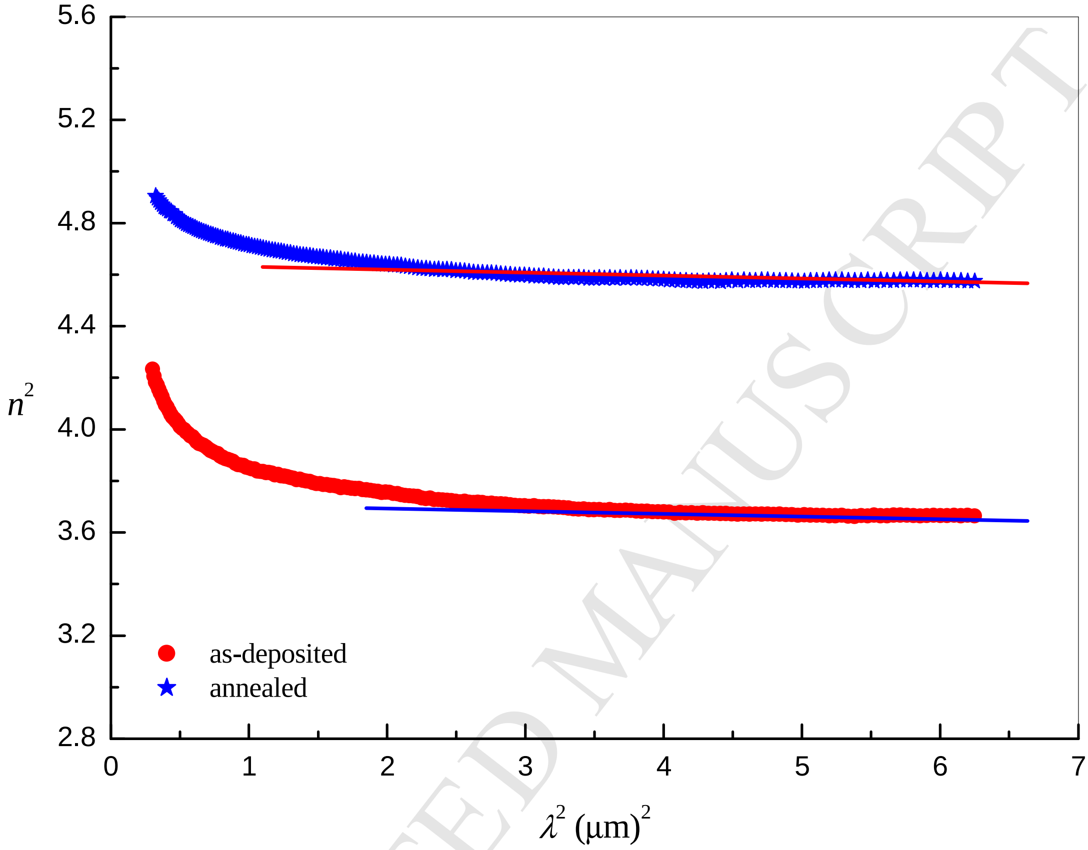

5.6
5.2
4.8
4.4
4.0
3.6
3.2
2.8
n^2
0
1
2
3
4
5
6
7
λ^2 (μm)^2
as-deposited
annealed

Fig. 7

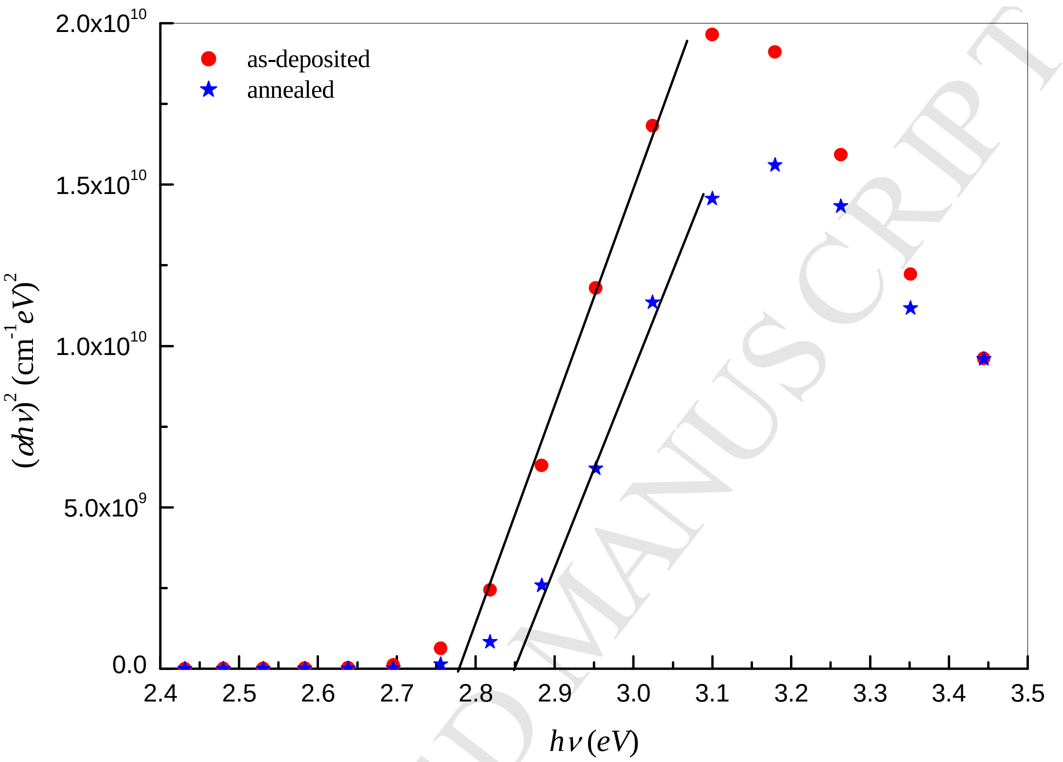
2.0x10^10
1.5x10^10
1.0x10^10
5.0x10^9
0.0
as-deposited
annealed
(αhν)^2 (cm^-1 eV)^2
2.4
2.5
2.6
2.7
2.8
2.9
3.0
3.1
3.2
3.3
3.4
3.5
hν (eV)

Fig. 8

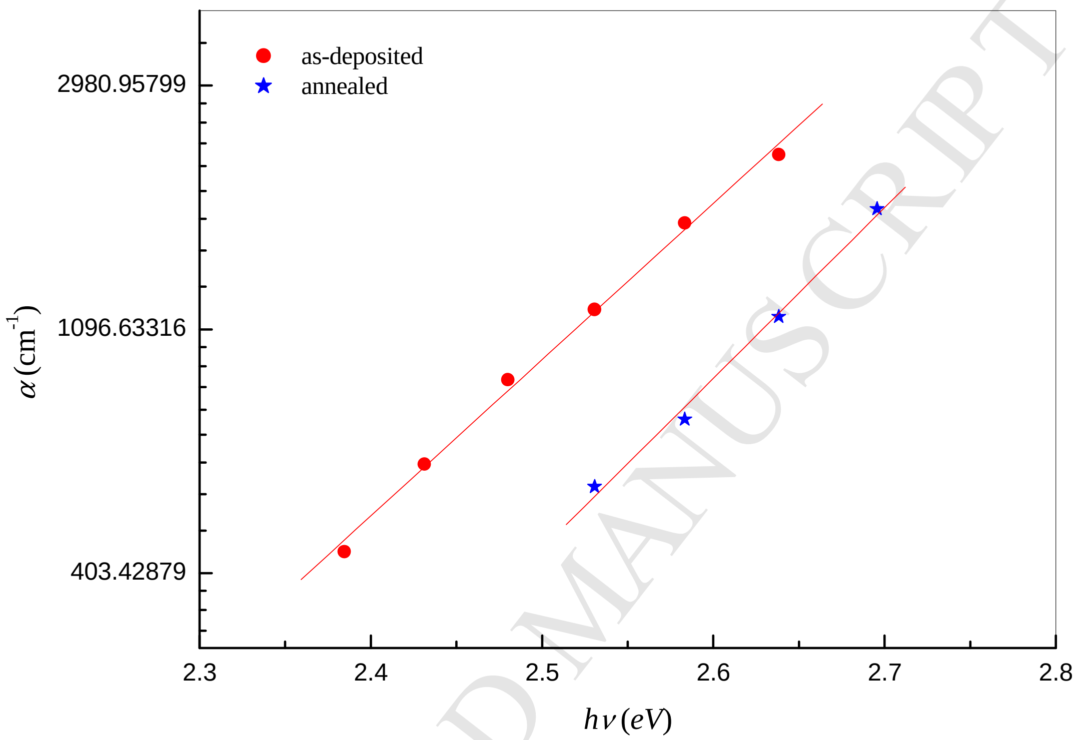
as-deposited
annealed
2980.95799
1096.63316
403.42879
$\alpha\,(\mathrm{cm}^{-1})$
2.3
2.4
2.5
2.6
2.7
2.8
$h\nu\,(eV)$

Fig. 9

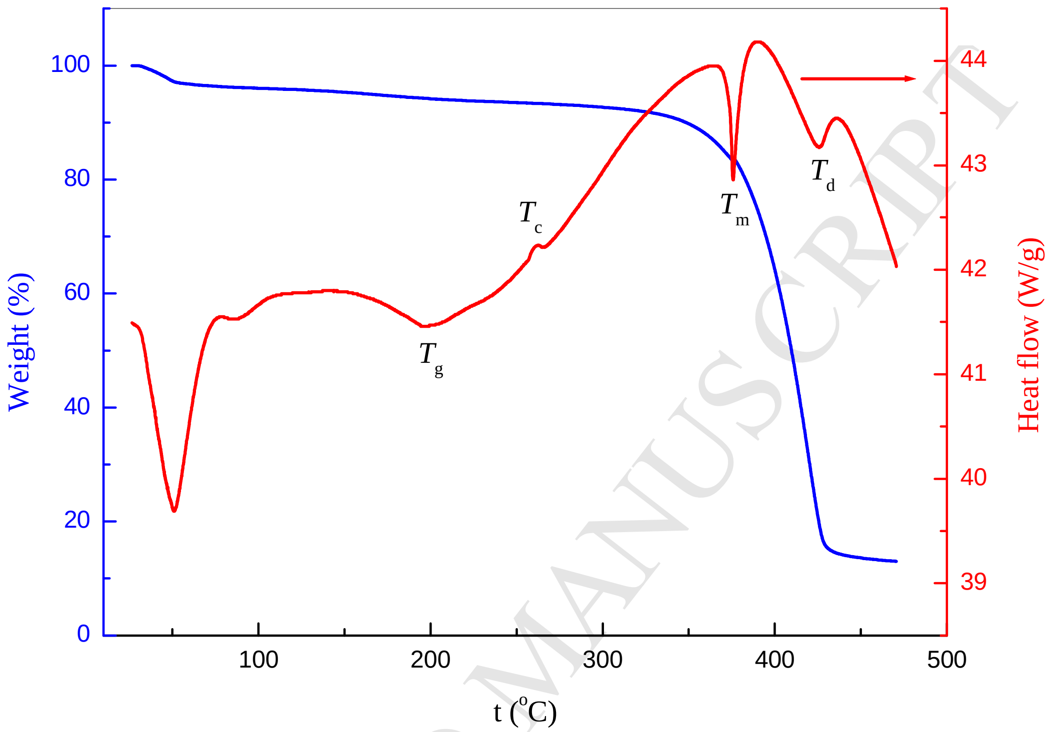

Weight (%)
0
20
40
60
80
100
Heat flow (W/g)
39
40
41
42
43
44
100
200
300
400
500
t (°C)
T g
T c
T m
T d

Fig. 10

► As-deposited amorphous Inq_3 films transform to crystalline upon annealing.

►The influence of annealing on optical properties of Inq_3 films is investigated.

►XRD and SEM is used to identify the structural properties.

►Single oscillator and Drude models are used to analyze the refractive index.

►The absorption edge is analyzed for determining the optical band gap.